Flux creep and penetration in Fe-doped $YBa_2Cu_3O_7$

M. A.-K. Mohamed, J. Jung, and J. P. Franck
Department of Physics, University of Alberta, Edmonton, Alberta, Canada T6G 2J1
(Received 6 April 1989; revised manuscript received 28 September 1989)

Measurements of the magnetic-field distribution, flux penetration, and decay of trapped flux were performed for a disc-shaped sample of $YBa_2Cu_{2.95}Fe_{0.05}O_{7-\delta}$ at 77 K. Time-dependent magnetic-flux penetration, i.e., a decay of diamagnetic shielding and the Meissner field, was observed for zero-field-cooled (ZFC) and field-cooled (FC) samples. The decays were found to be logarithmic in time. The logarithmic decay rate of diamagnetic shielding depends on an applied magnetic field and reaches its maximum at an applied field of about 30 G. The dependence of a trapped field versus an applied field shows a maximum at an applied field of 100 G for the FC case and 200 G for the ZFC case. The maximum amount of the trapped field is about two times less than that for a pure, undoped $YBa_2Cu_3O_{7-\delta}$ sample of similar dimensions. The logarithmic decay rate of the trapped field versus the initial trapped field is described by a linear function with the change of its slope at the trapped field corresponding to an applied field of about 30 G for both the FC and ZFC cases. These results are related to the sample microstructure, i.e., grain size and porosity. Trapped field decays can be explained in terms of the interaction between intergranular vortices and persistent current circulating around normal regions or voids, in the framework of the conventional flux-creep model recently proposed by Hagen, Griessen, and Salomons [Physica **157C**, 199 (1989)].

I. INTRODUCTION

Magnetic-flux pinning, flux motion, and its decay in high-temperature superconductors have been studied mainly by SQUID magnetometry,[1-7] torque techniques,[8,9] and high-resolution Bitter patterns.[10] These studies revealed that magnetic fields substantially less than 100 G can penetrate into $YBa_2Cu_3O_{7-\delta}$ superconducting ceramics due to weak connections between grains in polycrystalline samples. The presence of defects like grain boundaries, twinning planes, normal regions, and voids is responsible for very effective flux pinning. Trapped flux and persistent currents circulating around voids or nonsuperconducting regions contribute to the remanent magnetization present in these ceramic superconductors.

Understanding these properties requires a description of the magnetic structure of granular superconducting ceramics, including the spatial distribution of the magnetic field across the sample, the nature of flux penetration and pinning, time decays of trapped flux, and their response to changes of applied magnetic field. In this paper we report studies of the magnetic properties of Fe-doped $YBa_2Cu_3O_{7-\delta}$. Fe introduced into $YBa_2Cu_3O_{7-\delta}$ reduces its orthorhombic distortion[11] and lattice parameter along the c axis[12,13] as a result of substitution on the Cu and Ba sites.[14,11-13] As the result of these properties, superconducting ceramics of $YBa_2Cu_{3-x}Fe_xO_{7-\delta}$ contain more defects than those of $YBa_2Cu_3O_{7-\delta}$, their granular structure being characterized by small grain size and large porosity. On the other hand, the superconducting transition temperature of $YBa_2Cu_{3-x}Fe_xO_{7-\delta}$ decreases slowly with x_{Fe}, reaching $T_c \simeq 80-86$ K at $x_{Fe}=0.1$.[12,13]

One can, therefore, expect enhanced flux pinning, persistent currents circulating around voids or normal regions, and interaction between vortices and persistent current that could influence the creep of magnetic flux trapped in $YBa_2Cu_{3-x}Fe_xO_{7-\delta}$. We have studied the magnetic properties of Fe-doped $YBa_2Cu_3O_{7-\delta}$ for both zero-field-cooled and field-cooled samples. We measured the distribution of the magnetic field across the disc-shaped sample in the presence of an applied external magnetic field (up to 1000 G) and when the applied field was removed, the magnetic field dependence and time dependence of flux penetration and the trapped flux creep. We discuss the results obtained, taking into account the sample microstructure, i.e., the presence of normal regions or voids and their influence on the mechanism of the flux penetration and the time decay of trapped flux.

II. EXPERIMENTAL PROCEDURE

The measurements were performed on a disc-shaped sample of $YBa_2Cu_{2.95}Fe_{0.05}O_{7-\delta}$. The sample was prepared by the solid-state reaction method from metal oxides: Y_2O_3 (99.99% purity), CuO (99.999% purity), Fe_2O_3 (99.999% purity), and barium carbonate $BaCO_3$ (99.995% purity). The powders were mixed, ground, formed into a pellet, and reacted at 900 °C for 24 h. The product was recrushed, reground, formed into a disc-shaped sample (15 mm in diameter and 2.5 mm thick) under a pressure of 7300 bars and sintered in flowing oxygen at 925 °C for 7 h. The pellet was furnace cooled at the initial rate of 200 °C per hour. The sample has granular structure with a grain size around 1–3 μm and contains a large amount of voids (size around 1–3 μm) as ob-

FIG. 1. SEM photograph showing the grain structure and voids present in $YBa_2Cu_{2.95}Fe_{0.05}O_{7-\delta}$. The scale bar marks 5 μm.

served by scanning electron microscopy (Fig. 1). These voids occupy about 13% of the sample volume as determined by the measurement of the sample volume and weight. The superconducting transition temperature at zero resistance was found to be 90.3 K (Fig. 2). The width of the superconducting transition is 1 K. ac-susceptibility measurements gave a T_c of 89.7 K.

The magnetic properties of the sample, i.e., the magnetic-field distribution, magnetic-flux penetration, and time decays of the trapped field were measured at 77 K with an axial cryogenic Hall probe (sensitivity ± 0.030 G) which was scanned along a diameter of the disc-shaped sample. The sensitive area of the probe was equal to 0.44 mm^2. The axial probe measured the component of the magnetic field perpendicular to the disc-shaped sample at a distance of about 1 mm from the sample surface. The probe was connected to a gaussmeter and a computer-controlled system, which also allowed measurements of fast time decays of magnetic flux. A solenoid was used to generate magnetic fields in a direction perpendicular to the disc plane.

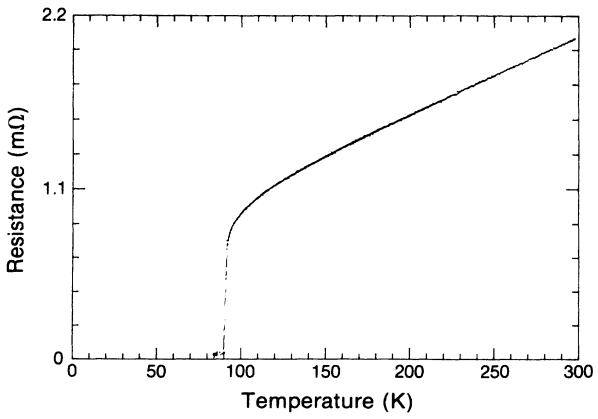

FIG. 2. Resistance vs temperature curve. Zero-resistance transition temperature equals 90.3 K.

III. EXPERIMENTAL RESULTS

Measurements of the distribution of the magnetic field across the sample, the dependence of flux penetration on the magnetic field and time, and time-dependent decay of the trapped flux have been performed for zero-field-cooled and field-cooled samples at 77 K. We have analyzed each case separately.

A. Zero-field-cooling case

Magnetic-field distributions measured across the disc-shaped sample for different external applied fields are shown in Figs. 3(a)–3(d). Upper curves show the distribution of the magnetic field measured in the presence of an external magnetic field over a range from 20 to 150 G after zero-field cooling. These curves represent the diamagnetic shielding. Lower curves show the distribution of the trapped magnetic field measured across the disc after the external magnetic field was switched off. The asymmetry observed for the flux distribution is mainly due to local nonuniformities of the sample. The magnetic-field distributions revealed the penetration of the magnetic flux into the disc from the perimeter towards its center at applied fields of up to 30–40 G. Below this field the trapped flux is mostly pinned along the disc perimeter.

The dependence of the diamagnetic shielding field measured at the disc center on an applied magnetic field is presented in Fig. 4. The shielding field exhibits a maximum at an applied field of around 20 G.

We observed a time-dependent decay of the diamagnetic shielding. The fine dotted curves in Fig. 3 represent the diamagnetic shielding (the upper curve) measured after waiting more than 60 000 s and the trapped field (the lower curve) that remained in the sample after the external magnetic field was reduced to zero at that time. The dependence of the diamagnetic shielding on time measured for different applied fields at the disc center is shown in Fig. 5. These decays are logarithmic in time. The logarithmic decay rate depends on the applied magnetic field (Fig. 6) showing a maximum at an applied field around 30 G. Below 15 G and above 100 G the diamagnetic shielding is nearly time independent.

The magnitude of the trapped field measured at the disc center was found to depend on an applied magnetic field (Fig. 7). It shows a maximum of 20 G at 150–200 G of the applied field. Figure 8 shows decays of the trapped field. These decays are also logarithmic in time. The logarithmic decay rate as a function of the initial trapped magnetic field (corresponding to an applied field up to 150 G) can be described by a linear function with the change of its slope at the trapped field of about 8 G, corresponding to an applied field of about 30 G (Fig. 9). The dependence of the decay rate on the trapped field below 8 G corresponds to that measured for the undoped $YBa_2Cu_3O_{7-\delta}$ superconductor.[15]

B. Field-cooling case

Distributions of the magnetic field measured across the disc-shaped sample for different external magnetic fields are presented in Figs. 10(a)–10(f). The upper curves

show the magnetic field distribution measured in the presence of external magnetic field over a range from 20 to 150 G after field cooling. These curves therefore represent the Meissner effect, which is stronger along the disc perimeter in external applied fields up to 40 G. The lower curves show the distribution of the trapped magnetic field after the external magnetic field was reduced to zero.

The dependence of the maximum Meissner field measured at the disc edge [see Fig. 10(a)–10(d)] on an applied magnetic field is shown in Fig. 11. The Meissner field exhibits a weak maximum at an applied field of around 40 G after which it increases much slower.

Time decay of the Meissner field measured at the disc center was observed for different applied fields (Fig. 12). Decays of the Meissner field are logarithmic in time. The logarithmic decay rates do not depend on the applied magnetic field and are quite small. Their value is approximately 0.2×10^{-1} G/decade, similar to those values observed for the decay of the shielding field below 15 G and above 100 G of applied field.

The magnitude of the trapped field measured at the disc center was found to depend on the applied magnetic field (Fig. 13). It shows a maximum at an applied field around 50 G. Figure 14 shows decays of the trapped field for different applied fields. These decays are also logarithmic in time. The logarithmic decay rate as a function of the initial trapped field (corresponding to an applied field up to 50 G) can be described (similarly to the zero-field cooling case) by a linear function with the change of its slope at a trapped field of about 16 G, which corresponds to an applied field of about 30 G (Fig. 15). The slope of this function below 16 G is about 30% of the corresponding slope for the logarithmic decay rate versus the trapped field in the zero-field cooling case; above a trapped field of 16 G the slope is about two times larger than in the zero-field-cooling case (Fig. 9).

The logarithmic decay rate of the trapped field versus

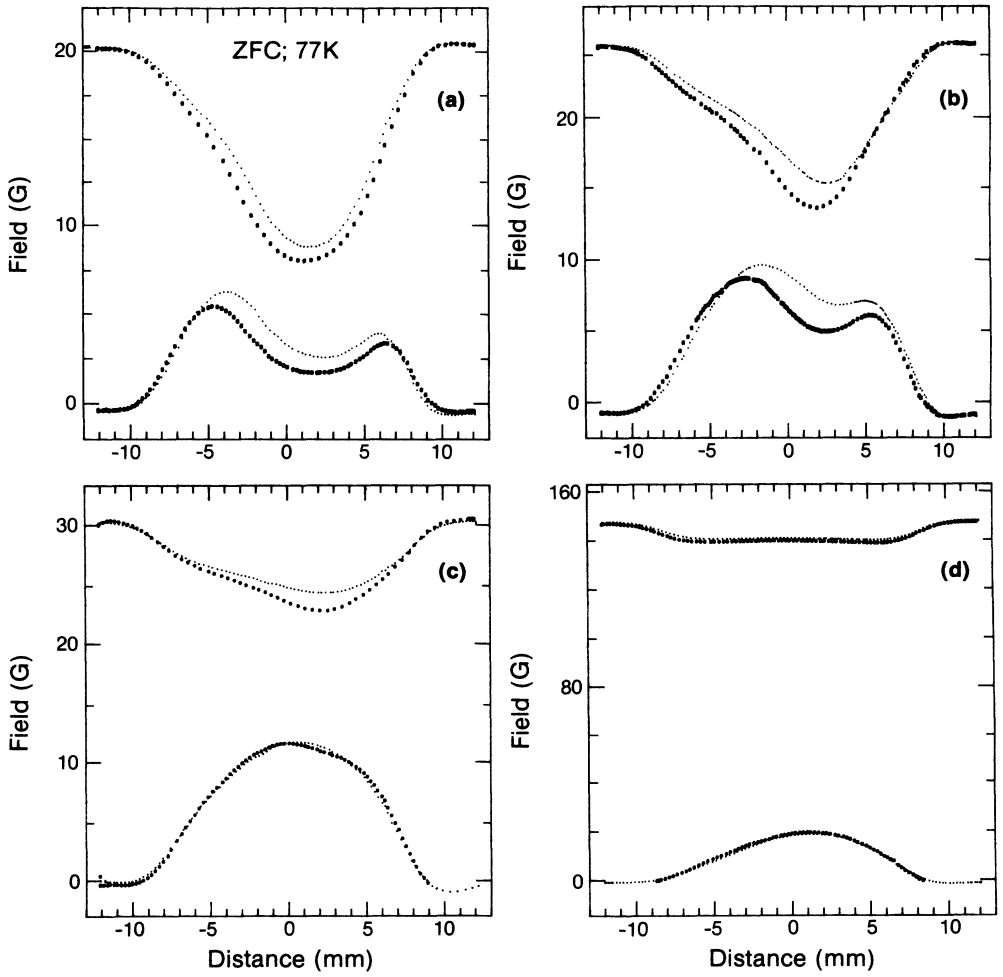

FIG. 3. Magnetic-field distribution for the zero-field-cooled disc-shaped sample of $YBa_2Cu_{2.95}Fe_{0.05}O_{7-\delta}$ measured for different applied magnetic fields at 77 K: (a) 20.6 G, (b) 25 G, (c) 30 G, and (d) 146 G. The upper curves show the diamagnetic shielding (applied field present). The lower curves show the trapped field (applied field reduced to zero). The fine-dotted upper curves show the diamagnetic shielding measured after a waiting time of more than 6×10^4 s. The fine-dotted lower curves show the corresponding trapped field measured at that time. Modifications of the shielding field due to the vortex formation near the edges of the sample can be seen. Distances -7.5 mm and $+7.5$ mm mark the disc edges.

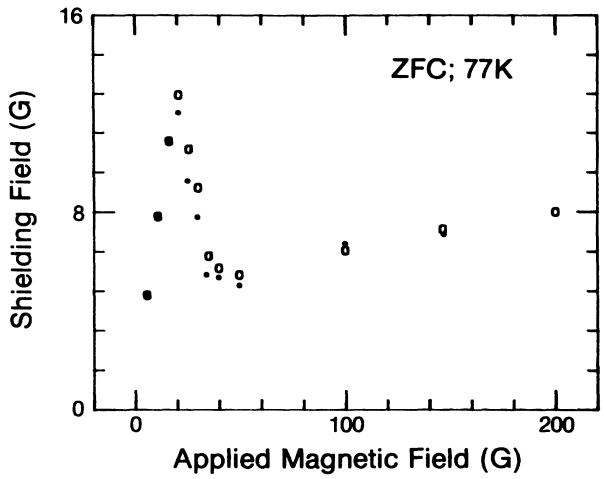

FIG. 4. The shielding field vs the applied magnetic field measured for the zero-field-cooled sample at the disc center (open symbols). The dots represent the shielding field measured after 60 000 s.

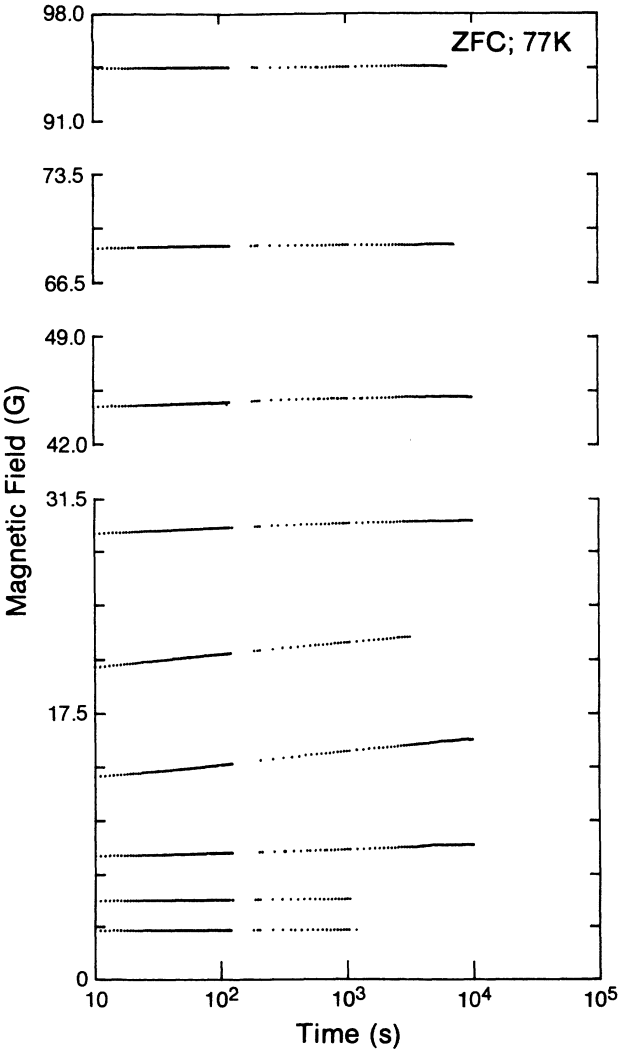

FIG. 5. Time decays of the diamagnetic shielding field measured at the disc center for the zero-field-cooling case. These decays are logarithmic in time.

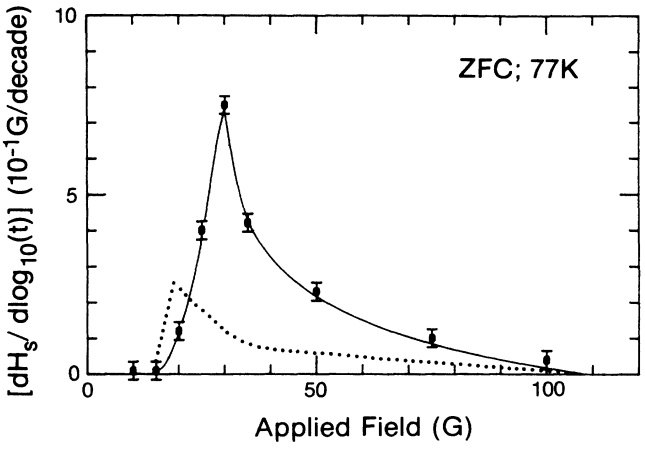

FIG. 6. The dependence of the shielding field decay rate on the applied magnetic field for the zero-field-cooling case. The dotted line shows the shielding decay rate for a ring-shaped sample (I.D. 3 mm, O.D. 15 mm) of pure $YBa_2Cu_3O_{7-\delta}$.

the applied magnetic field for both zero-field-cooling and field-cooling cases are shown in Fig. 16. The decay rates are nearly independent of the method of sample cooling for the applied field below 30 G. Above this field, the decay rates for the field-cooling case are higher than the corresponding decay rates for the zero-field-cooling case.

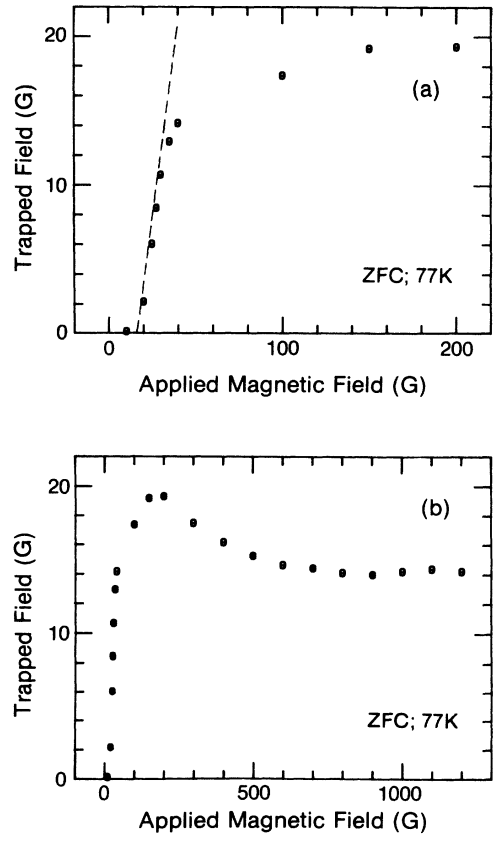

FIG. 7. The dependence of the trapped field measured at the disc center on an applied magnetic field for the zero-field-cooling case: (a) applied fields up to 200 G and (b) applied fields up to 1200 G.

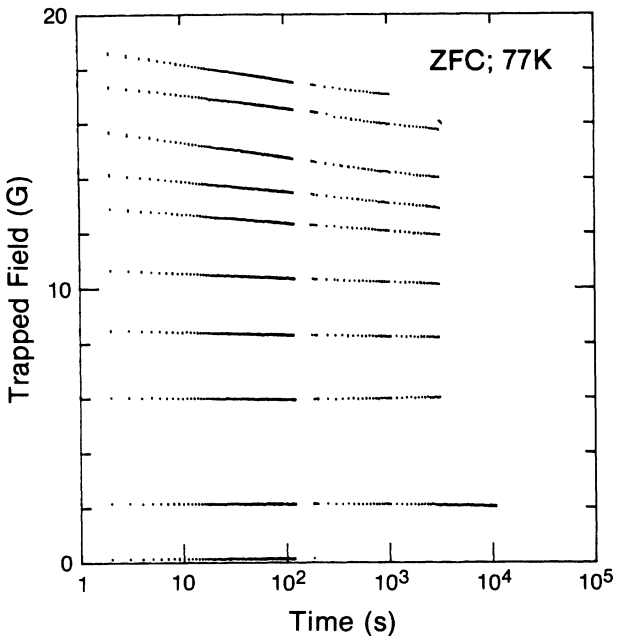

FIG. 8. Time-decays of the trapped magnetic field measured at the disc center of the zero-field-cooling case. These decays are logarithmic in time.

IV. DISCUSSION

We discuss next the relationship between the microstructure of the Fe-doped $YBa_2Cu_3O_{7-\delta}$ sample and the observed time decays of the diamagnetic shielding and of the trapped flux. We explain how the dependence of the trapped flux decay rate on an applied magnetic field (0–1000 G range) can be understood in a flux-creep model proposed recently by Hagen *et al.*,[16] and in terms of the interaction between intergranular vortices and the persistent currents circulating around voids or nonsuperconducting regions. We analyze the time decay of diamagnetic shielding and the time decay of the trapped flux separately.

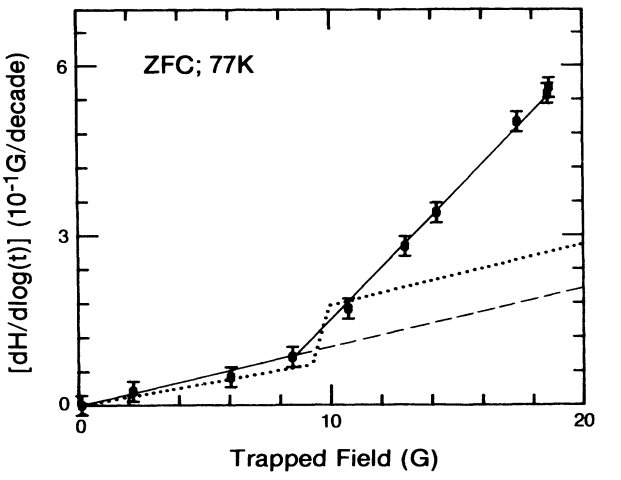

FIG. 9. Dependence of the trapped-field decay rate on the initial trapped field measured for the zero-field-cooling case. The dotted line shows the trapped field decay rate for a ring-shaped sample of pure $YBa_2Cu_3O_{7-\delta}$ (I.D. 3 mm, O.D. 15 mm). The dashed line represents the trapped field decay rate measured for a disc-shaped sample of $YBa_2Cu_3O_{7-\delta}$ for both the ZFC and FC cases.

A. Magnetic-field distribution in the ZFC and FC cases

In the zero-field-cooling case both the shielding and the trapped field are nonuniform at low fields. The shielding is maximum in the center of the disc and less towards the edges; correspondingly, the trapped field is larger at the edges. The shielding field for applied fields above 20 G shows modifications near the edges of the sample, which are likely due to vortex formations [see Figs. 3(a)–3(c)]. These distributions are due to the large demagnetization effect at the edges of a low-aspect-ratio cylinder.[17,18] Similar results were also observed in our earlier studies on unsubstituted $YBa_2Cu_3O_{7-\delta}$ discs.[15] For low magnetic fields the trapped field is larger at the edges of the $YBa_2Cu_3O_{7-\delta}$ disc. The trapped field produces one uniform peak at the center of the disc for applied fields higher than 45 G. In the Fe-doped $YBa_2Cu_3O_{7-\delta}$ this happens for applied fields higher than 30 G [Fig. 3(c)]. Larger demagnetization effects in the $YBa_2Cu_{2.95}Fe_{0.05}O_{7-\delta}$ disc due to larger porosity and penetration depth are responsible for the penetration of magnetic flux at smaller applied fields.

In the field-cooling case we observe a partial Meissner effect. At low applied fields, the Meissner expulsion is largest near the edges of the disc; for larger applied fields the maximum Meissner expulsion moves towards the center. This effect can also be understood as being due to the large and nonuniform demagnetization near the edges of the disc. This leads to a gradient in the internal field, and a consequent motion and loss of flux lines through the edges. These effects are also similar to those observed in our work on unsubstituted $YBa_2Cu_3O_{7-\delta}$ (Ref. 15) (in the case of the $YBa_2Cu_3O_{7-\delta}$ disc the demagnetization effects at its edges are smaller and the Meissner exclusion is uniform across the disc) and in the work by Dolan *et al.*[10] on $YBa_2Cu_3O_{7-\delta}$ using the high-resolution Bitter-pattern technique.

B. Time decays

Whereas the field distribution for both the zero-field and field-cooling case in the Fe-doped samples is very similar to those observed in a pure $YBa_2Cu_3O_{7-\delta}$ disc, we observed characteristic differences in the time decay of both the shielding field and of the trapped fields. In particular the shielding field decays with time for the intermediate applied field range between 15 and 100 G; this was not observed in a pure $YBa_2Cu_3O_{7-\delta}$ disc. Moreover, we observed characteristic changes in the rate of time decay of the trapped field at an applied field near 30 G (corresponding to trapped fields of 8 G for the ZFC case and 16 G for the FC case). An indication of the possible reason for these different behaviors was obtained

when we investigated the magnetic behavior of a ring of pure $YBa_2Cu_3O_{7-\delta}$ material.[19] When the pure $YBa_2Cu_3O_{7-\delta}$ disc was changed into a ring by drilling a 3-mm hole through its center, we observed qualitatively very similar time dependences as described here for the Fe-substituted disc. In particular, we also observed time dependence of the shielding field in the same applied field regions as observed here (Fig. 6); we also find the characteristic changes in the rate of the trapped field decay at low fields (Figs. 9 and 15).[19] These coincidences in behavior are remarkable, and point to the fact that the time-decay behavior in the Fe-doped disc is essentially a geometric effect, in particular, due to the existence of multiply connected regions. Such regions exist in the Fe-doped material due to the presence of normal regions or voids (Fig. 1).

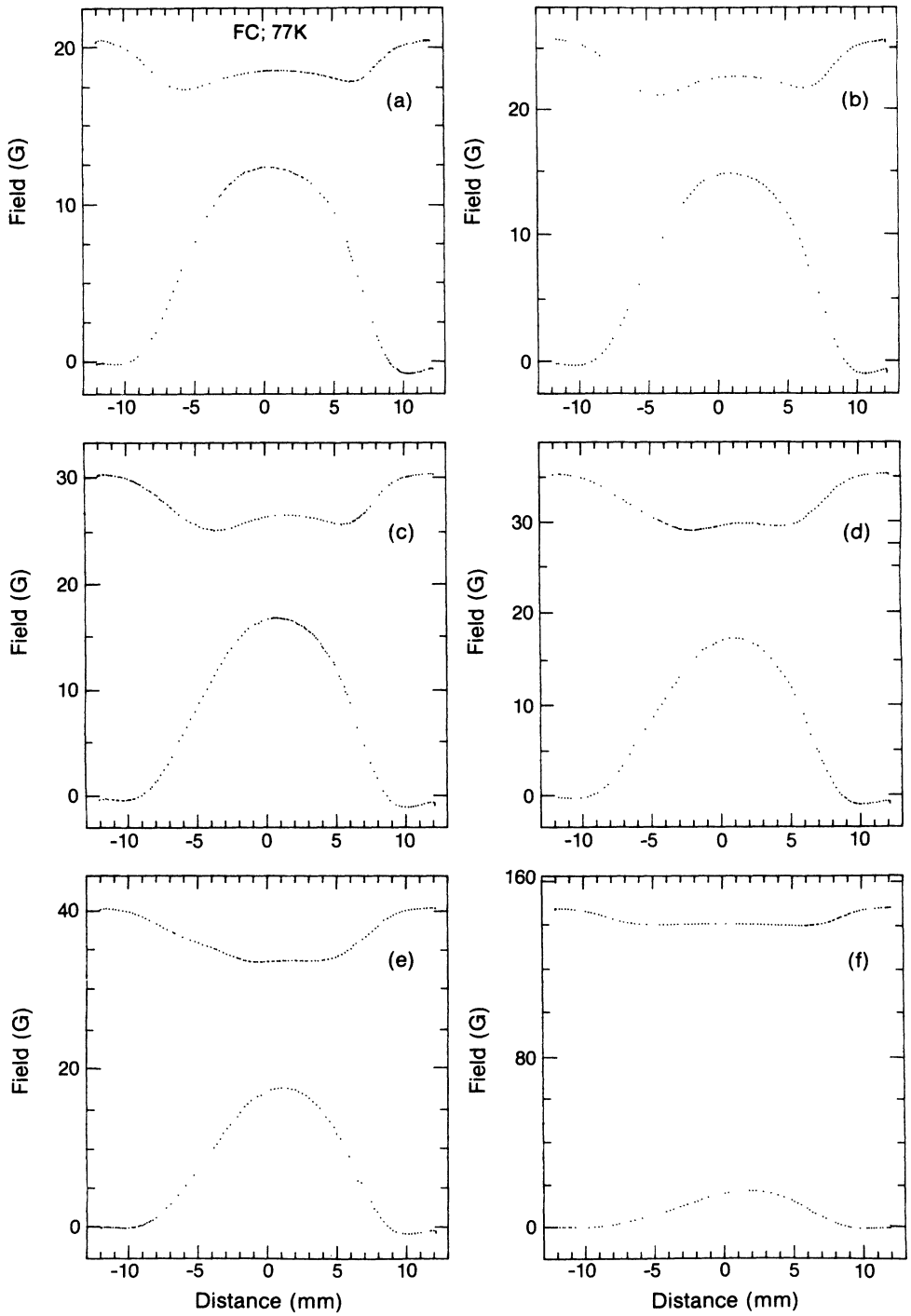

FIG. 10. Magnetic-field distributions for the field-cooled disc-shaped sample of $YBa_2Cu_{2.95}Fe_{0.05}O_{7-\delta}$ measured for different applied magnetic fields at 77 K: (a) 20 G, (b) 25 G, (c) 30 G, (d) 35 G, (e) 40 G, and (f) 146 G. The upper curves show the Meissner effect (applied field present). The lower curves show the trapped field (applied field reduced to zero). Distances −7.5 mm and +7.5 mm mark the disc edges.

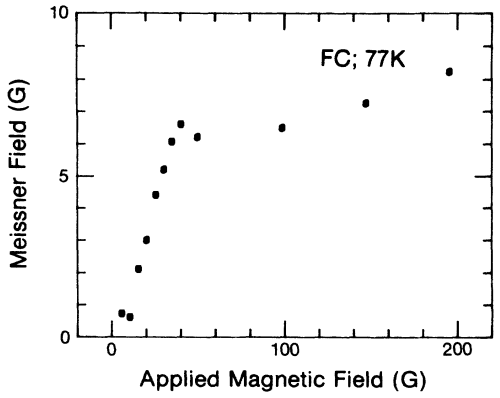

FIG. 11. The dependence of the maximum Meissner field on the applied magnetic field measured for the field-cooled sample.

1. *Time decay of diamagnetic shielding*

In Fig. 4 we show the shielding field as a function of the applied field. At an applied field of about 20 G we observe a pronounced maximum in the shielding field, a similar maximum was also found in the pure $YBa_2Cu_3O_{7-\delta}$ disc results.[15,19] Apparently at this stage a critical point is reached for the shielding current passing through weak links interconnecting the grains. For larger fields, vortices will be created in enclosed regions, the field produced by these is visible as small deviations from the smooth shielding curve for applied fields larger than 20 G in Fig. 3. The effect is most pronounced near the edges because of demagnetization effects. The decay of shielding apparently is caused by the motion of these vortices. For the Fe-doped disc of this study the vortices can be thought to move towards voids or normal regions in the material, in the ring of the $YBa_2Cu_3O_{7-\delta}$ compound they move towards the central hole. This motion is caused by large local-field gradients near voids or normal regions. When the vortices are close to these regions shielding currents exceed their critical value. This allows fluxons to leak into these regions. The effect is largest when the vortices are first created, and is becoming smaller again at larger fields, when the vortex density becomes larger, and the local-field gradients are reduced. This interpretation receives further support from our observation that the decay of the Meissner field in the field-cooling case shows no applied field dependence. In this case the field already fills all voids and normal regions and the local-field gradients are insufficient to move the vortices.

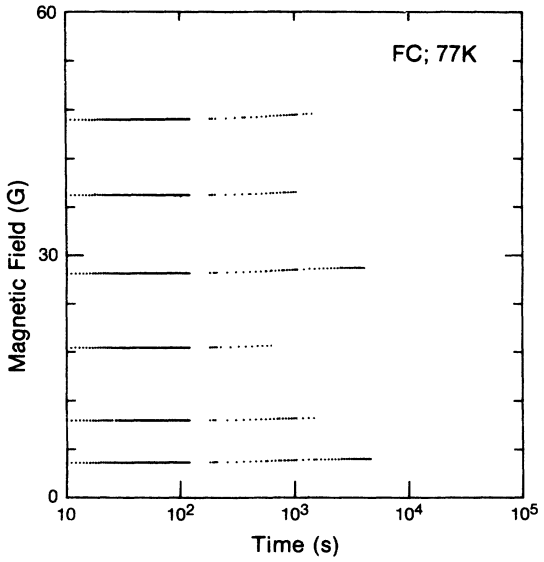

FIG. 12. Time decays of the Meissner field for the field-cooling case. These decays are logarithmic in time and are independent of the applied magnetic field.

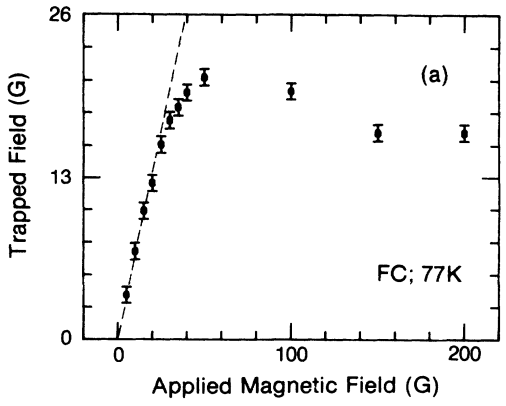

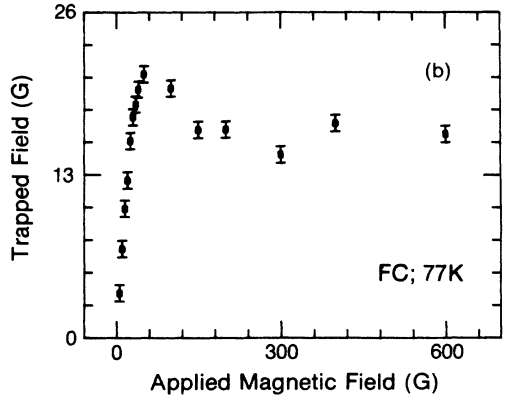

FIG. 13. Dependence of the trapped field measured at the disc center on an applied magnetic field for the field cooling case: (a) applied field up to 200 G and (b) applied field up to 600 G.

2. *Time decay of the trapped flux*

The trapped field observed both in the zero-field and field-cooling cases is composed of contributions from trapped intergranular vortices and from persistent currents circulating around voids or normal regions.

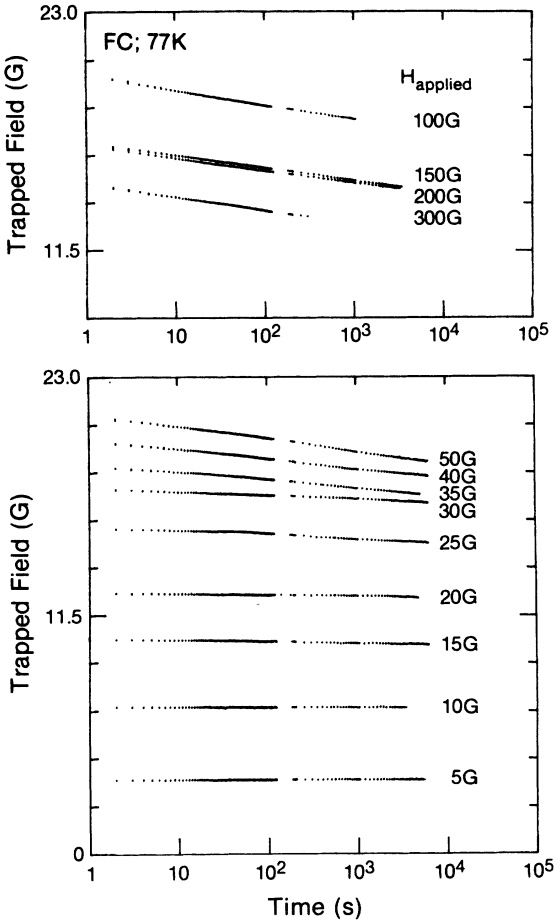

FIG. 14. Time decays of the trapped field measured at the disc center for the field-cooling case as a function of the applied field. These decays are logarithmic in time.

From Figs. 7 and 13 we see that the maximum trapped field is near 20 G in both the zero-field and field-cooling cases. In the former case this trapped field is reached for an applied field of 150 G, and in the field-cooling case for 80 G. This maximum trapped field coincides with the applied field at which the maximum shielding is observed

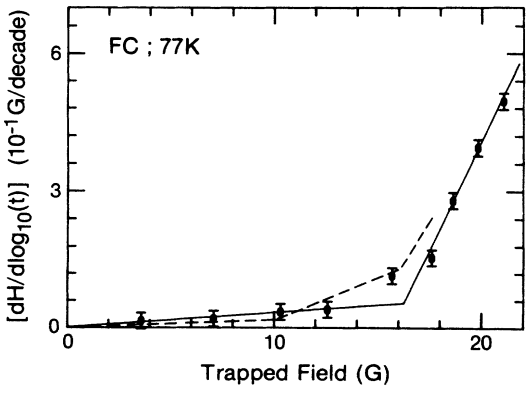

FIG. 15. Dependence of the trapped field decay rate on the initial trapped field measured for the field-cooling case. The dashed line represents the trapped field decay rate for a ring-shaped sample of $YBa_2Cu_3O_{7-\delta}$ (I.D. 3 mm, O.D. 15 mm).

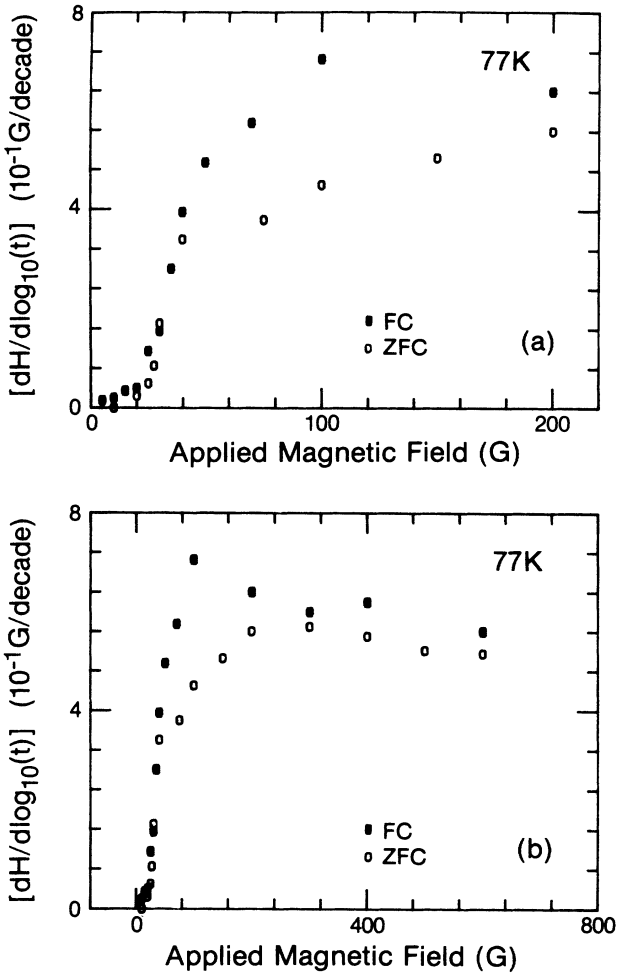

FIG. 16. Dependence of the trapped field decay rate on the applied magnetic field measured for the field-cooling case (solid symbols) and the zero-field-cooling case (open symbols): (a) applied field up to 200 G and (b) applied field up to 600 G.

(Fig. 4). At this field the persistent currents contributing to the trapped field start to become smaller again due to decoupling of grains. Applied fields causing decoupling of grains were also observed by Nikolo and Goldfarb[20] in $YBa_2Cu_3O_{7-\delta}$ compounds; values between 13 and 25 G are cited. For a disc-shaped sample of $YBa_2Cu_3O_{7-\delta}$ the trapped field achieves its saturation value for applied fields above 200 G for the FC case and 350 G for the ZFC case.[15] Cutting a ring out of a disc-shaped sample of $YBa_2Cu_3O_{7-\delta}$ results also in a maximum of the trapped field observed at applied fields of 100–150 G for the FC case[19] and at 150–200 G for the ZFC case.[19]

The time decay of the trapped magnetic field observed in high-temperature superconductors either after zero-field cooling or field cooling was attributed to the presence of a glassy state[1,6,7] or to thermally activated flux creep[4,5,21] Thermally activated flux creep was believed to be the result of the small coherence length that leads to an unusually low pinning energy[5] and the high temperature at which flux-creep experiments are performed (about 77 K). The theory of thermally activated flux

creep was first proposed by Anderson.[22] This theory considers thermal activation of flux bundles over a barrier with activation energy E. A gradient in the density of flux bundles causes a driving force F to act on the flux bundles. Even if the local pinning force F_p is larger than F, flux creep is still possible with the help of thermal activation. The effective activation energy for thermally activated motion of a flux bundle is given by

$$E = E_0 - |\mathbf{F}| VX \ , \tag{1}$$

where E_0 is the height of the energy barrier, the term $|\mathbf{F}| VX$ represents the decrease in the barrier height due to driving force $\mathbf{F}$ (per unit volume) acting on the flux bundle, V is the flux bundle volume, and X is the effective geometrical width of the energy barrier. According to Anderson's theory the time dependence of the magnetization $M(t)$ follows a logarithmic law, i.e., $M(t) \sim \ln(t)$. Anderson's theory considers flux bundle movement from one pinning region to another through a thermally activated process in the limit $E_0/kT \gg 1$. This theory was extended by Hagen *et al.*[9] to flux motion in a solid consisting of many pinning regions. Time-dependent magnetization is given in the form

$$M(t) \simeq M(0) \left[1 - \frac{kT}{E} \ln \left[1 + \frac{t}{t_0} \right] \right] , \tag{2}$$

where t_0 is a characteristic time depending on the number of pinning regions and the activation energy E.

The logarithmic decay rate (for times $t \gg t_0$) is proportional to the initial magnetization $M(0)$ and inversely proportional to the activation energy E,

$$\frac{dM(t)}{d\ln t} = -M(0) \frac{kT}{E} \ . \tag{3}$$

The results of our experiments show the linear dependence of logarithmic decay rate of the trapped field on the initial value of the trapped field. The slope of the linear function allowed us to calculate the activation energy of a flux-creep process. The decay rate of the trapped field versus the trapped field measured on a disc-shaped sample of $YBa_2Cu_3O_{7-\delta}$ for applied fields below 1000 G can be described by a linear function up to a maximum trapped field that is equal to about 40 G.[15] This decay rate was observed to be the same for zero-field cooling and field-cooling cases and is represented by a straight dashed line in Fig. 9. The corresponding flux-creep activation energy E was calculated to be about 1.6 ± 0.3 eV at 77 K. This value is close to flux-creep activation energies found for conventional type-II superconductors, e.g., for PbTl alloys $E \sim 1$ eV in low fields.[23]

The logarithmic decay rate of the trapped field measured versus the initial trapped field for Fe-doped $YBa_2Cu_3O_{7-\delta}$ is described by a linear function with the change of its slope at the trapped field 8 G for the ZFC case and at 16 G for the FC case, both trapped fields corresponding to an applied field of about 30 G. It is interesting to note that cutting a ring out of a disc-shaped sample of $YBa_2Cu_3O_{7-\delta}$ also causes similar dependence of the trapped field decay rate on the initial trapped field (see Figs. 9 and 15). In both cases the change of the slope means lower activation energies for the flux creep. These experiments lead to the conclusion that the interaction between the intergranular vortices and the persistent currents circulating around the voids or nonsuperconducting regions in a sample is the reason for the observed change in the time-decay rate of the trapped field, suggesting that persistent currents provide a driving force acting on flux bundles.

For Fe-doped $YBa_2Cu_3O_{7-\delta}$ zero-field cooled sample, at trapped fields below 8 G, the activation energy for flux motion is 1.7 ± 0.2 eV, close to that for the disc-shaped sample of $YBa_2Cu_3O_{7-\delta}$ (1.6 ± 0.3 eV). The trapped field of 8 G corresponds to an applied field of 30 G at which the whole sample is filled with intergranular vortices (see Fig. 3). Above 30 G a rigid vortex intergranular lattice is present in the sample; below 30 G the motion of vortices towards the center of the disc suggests the existence of a "soft" intergranular vortex distribution [Figs. 3(a) and 3(b)]. The formation of an intergranular rigid vortex lattice in $YBa_2Cu_3O_7$ at low fields has been observed by Dolan *et al.*[10] When the applied field is reduced to zero we have an additional contribution to the trapped field due to persistent currents generated around voids or normal regions. In the presence of a rigid vortex lattice interaction between the vortices and the persistent current takes place. The vortices experience a Lorentz force which decreases the effective activation energy for the flux creep to about 0.6 eV (Fig. 9).

Contribution of persistent currents to the trapped field for the field-cooled Fe-doped samples is larger than in the case of the zero-field-cooled samples (Figs. 7 and 13). At the trapped field of 16 G (which corresponds to an applied field of 30 G as in the ZFC case) strong interaction between a rigid intergranular vortex lattice and persistent currents takes place reducing the effective activation energy for flux motion down to 0.2 eV. There is no interaction between a "soft" intergranular vortex distribution and persistent currents at the trapped fields below 16 G. Since the persistent current does not contribute to the time decay of the trapped field as pointed out by Leiderer and Feile,[24] it decreases the slope of the decay rate of the trapped field measured versus the initial trapped field (Fig. 15). This interpretation receives further support from our observation of similar dependence of the trapped-field decay rate measured versus the initial trapped field for a ring-shaped $YBa_2Cu_3O_{7-\delta}$ sample (Figs. 9 and 15).

V. CONCLUSIONS

The experiments performed for Fe-doped $YBa_2Cu_3O_{7-\delta}$, especially intergranular flux-creep measurements, support a conventional picture of thermally activated motion of a magnetic flux in type-II superconductors, at least in the high-temperature (77 K), low-field (0–100 G) range. The activation energy for thermal flux creep was calculated to be 1.7 ± 0.2 eV at applied fields below 30 G in agreement with activation energy for thermally activated flux motion in conventional type-II superconductors. This energy was found to be reduced to 0.2–0.6 eV at applied fields above 30 G due to the interac-

tion between trapped flux (intergranular vortices) and persistent currents that provide a driving force acting on vortices. The microstructure of superconducting ceramics and their inhomogeneity are responsible for the presence of persistent currents circulating around voids or nonsuperconducting regions in these materials.

ACKNOWLEDGMENTS

We would like to thank S. Gygax for ac-susceptibility measurements of our sample. This work was supported by grants from the Natural Sciences and Engineering Research Council of Canada.

[1]K. A. Müller, M. Takashige, and J. G. Bednorz, Phys. Rev. Lett. **58**, 1143 (1987).

[2]A. C. Mota, A. Pollini, P. Visani, K. A. Müller, and J. G. Bednorz, Phys. Rev. B **36**, 4011 (1987).

[3]A. P. Malozemoff, L. Krusin-Elbaum, D. C. Cronemeyer, Y. Yeshurun, and F. Holtzberg, Phys. Rev. B **38**, 6490 (1988).

[4]Y. Yeshurun, A. P. Malozemoff, F. Holtzberg, and T. R. Dinger, Phys. Rev. B **38**, 11 828 (1988).

[5]Y. Yeshurun and A. P. Malozemoff, Phys. Rev. Lett. **60**, 2202 (1988).

[6]M. Foldeaki, M. E. McHenry, and R. C. O'Handley, Phys. Rev. B **39**, 2883 (1989).

[7]C. Rossel, Y. Maeno, and I. Morgenstern, Phys. Rev. Lett. **62**, 681 (1989).

[8]C. Giovanella, G. Collin, P. Rouault, and I. A. Campbell, Europhys. Lett. **4**, 109 (1987).

[9]C. W. Hagen, M. R. Bom, R. Griessen, B. Dam, and H. Veringa, Physica **153-155C**, 322 (1988).

[10]G. L. Dolan, G. V. Chandrashekhar, T. R. Dinger, C. Field, and F. Holtzberg, Phys. Rev. Lett. **62**, 827 (1989).

[11]Y. Maeno, T. Tomita, M. Kyogoku, S. Awaji, Y. Aoki, K. Hoshino, A. Minami, and T. Fujita, Nature **328**, 512 (1987).

[12]H. Obara, H. Oyanagi, K. Murata, H. Yamasaki, H. Ihara, M. Tokumoto, Y. Nishihara, and Y. Kimura, Jpn. J. Appl. Phys. **4**, L603 (1988).

[13]J. Jung, J. P. Franck, W. A. Miner, and M.A-K. Mohamed, Phys. Rev. B **37**, 7510 (1988).

[14]B. D. Dunlap, J. D. Jorgensen, W. K. Kwok, C. W. Kimball, J. L. Matykiewicz, H. Lee, and C. V. Segre, Physica **153-155C**, 1100 (1988).

[15]M. A-K. Mohamed, J. Jung, and J. P. Franck, Phys. Rev. B **39**, 9614 (1989). (The magnetic fields and the decay rate quoted in this reference are in error. They should be multiplied by a factor of 10.)

[16]C. W. Hagen, R. P. Griessen, and E. Salomons, Physica **157C**, 199 (1989).

[17]D. Schoenberg, *Superconductivity* (Cambridge University Press, Cambridge, 1952), p. 22.

[18]U. Essmann, *Superconductivity—Proceedings of the International Conference on the Science of Superconductivity, Stanford, 1969* (North-Holland, Amsterdam, 1971), p. 83.

[19]M. A-K. Mohamed, J. Jung, and J. P. Franck, Phys. Rev. B (to be published).

[20]M. Nikolo and R. B. Goldfarb, Phys. Rev. B **39**, 6615 (1989).

[21]M. A-K. Mohamed, W. A. Miner, J. Jung, J. P. Franck, and S. B. Woods, Phys. Rev. B **37**, 5834 (1988).

[22]P. W. Anderson, Phys. Rev. Lett. **9**, 309 (1962).

[23]M. R. Beasley, R. Labusch, and W. W. Webb, Phys. Rev. **181**, 682 (1969).

[24]P. Leiderer and R. Feile, Z. Phys. B **70**, 141 (1988).

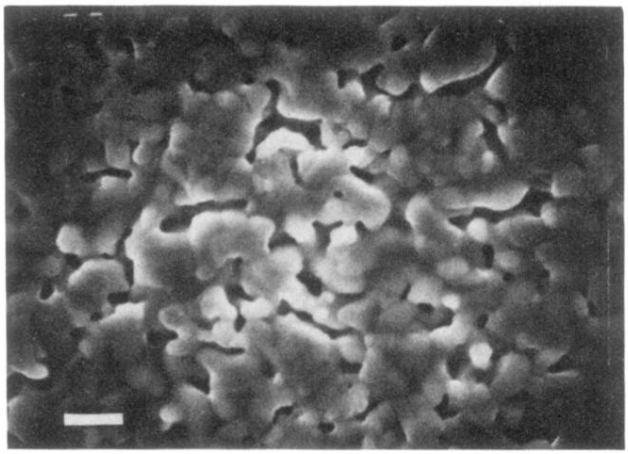

FIG. 1. SEM photograph showing the grain structure and voids present in $YBa_2Cu_{2.95}Fe_{0.05}O_{7-\delta}$. The scale bar marks 5 μm.